IC/93/62

INTERNATIONAL CENTRE FOR THEORETICAL PHYSICS

CO_2 LASER WITH MODULATED LOSSES: THEORETICAL MODELS AND EXPERIMENTS IN THE CHAOTIC REGIME

C. L. Pando L.

R. Meucci

M. Ciofini

and

F.T. Arecchi

INTERNATIONAL ATOMIC ENERGY AGENCY

UNITED NATIONS EDUCATIONAL, SCIENTIFIC AND CULTURAL ORGANIZATION

MIRAMARE-TRIESTE

IC/93/62

International Atomic Energy Agency
and
United Nations Educational Scientific and Cultural Organization
INTERNATIONAL CENTRE FOR THEORETICAL PHYSICS

CO_2 LASER WITH MODULATED LOSSES: THEORETICAL MODELS AND EXPERIMENTS IN THE CHAOTIC REGIME

C.L. Pando L.
International Centre for Theoretical Physics, Trieste, Italy

R. Meucci, M. Ciofini and F.T. Arecchi
Istituto Nazionale di Ottica,
Largo E. Fermi 6, 50125 Firenze, Italy.

ABSTRACT

We compare two different theoretical models for a CO_2 laser, namely the two- and four-level model, and show that the second one traces with much better accuracy the experimental behavior in the case of a chaotic dynamics due to time modulation of the cavity losses. Even though the two-level model provides a qualitative explanation of the chaotic dynamics, only the four-level one assures a quantitative fitting. We also show that, at the onset of chaos, the chaotic dynamics is low dimensional and can be described in terms of a noninvertible unidimensional map.

MIRAMARE - TRIESTE
April 1993

1.INTRODUCTION

The loss modulated single mode CO_2 laser is the first optical device where chaotic dynamics has been investigated in a detailed way, not limiting the chaotic evidence to irregular time patterns or broadened power spectra, but characterizing quantitatively the chaotic scenario by suitable indicators [1]. At the same time, a large effort has been done in providing the simplest exhaustive theoretical model for the CO_2 laser able to reproduce adequately the experiments [2,3,4,5]. The widely used approach based on two rate equations for the photon number n and the population inversion δ [1] (two-level model, 2LM) provides only a qualitative agreement with the experiments. In a recent paper [5] it has been shown that in a Q-switch experiment the main limitations of 2LM appear when the amplification regime is no more linear and saturation effects induced by the coupling between n and δ become relevant. More accurate results can be obtained by using the so-called four-level model (4LM) which takes into account the collisional coupling of each resonant energy level with a certain number of rotational levels of the same vibrational band.

The aim of this paper is to extend the analysis of Ref. 5 comparing the two different models with an experimental situation where nonlinearities play a fundamental role, that is, the chaotic dynamics obtained by applying a time modulation to the cavity losses.

In order to make a more complete comparison, we have considered two cases of 2LM. In the first (two-level model standard, or 2LMS) the value of the population decay rate γ to be considered in the rate equations is in the range of the values measured directly by spectroscopic techniques. As a

consequence, no agreement is reached between the measured and calculated saturation intensities. To account for this, a second model (two-level model equivalent, or 2LME) is considered, whereby the value of γ is derived by the requirement that the predicted value of saturation intensity should agree with the experimental one, and then γ results much higher (an order of magnitude) than the actual value.

Trying to fit all the experimental features of the chaotic dynamics with theoretical predictions, we will show that both two-level models give unrealistic results while the four-level model describes with a good degree of accuracy the experiment. 2LMS shows chaotic evolution for a range of modulation frequencies close to the experimental value but for much lower modulation amplitudes, while 2LME provides chaos for the correct range of modulation amplitudes but for higher modulation frequencies. 4LM is free of both drawbacks.

Besides the comparison between the theoretical models and the experimental results, we have investigated two experimental features that had received scarce attention beforehand, namely, the period bubbling behavior [6] and the unidimensional-map contraction of the laser dynamics at the onset of chaos [7]. In fact it was the analysis of 4LM which gave us indications for searching these experimental properties, which in turn are related with one another [8,9]. The period bubbling property that we find in our system refers to a sequence of period doublings followed by the inverse process as the modulation amplitude is kept constant and the modulation frequency is varied. Depending on the strength of the modulation amplitude the sequence of period doublings may not end into chaos giving

rise in this way to a big primary bubble within which higher order bubbles are contained [9]. Such a behavior has been found in other systems [8] and seems characteristic of low dimensional dynamics. This suggests that our system can be described by means of a noninvertible unidimensional map within a certain interval of parameter values, when the signal is chaotic. However these features do not appear for all parameter values since crises may take place [10,11]. Let us point out that generalized multistability found in lasers [1] is related to the existence of crises of attractor destruction-type, since it suggests the coexistence of different attractors. In other words, multistability may inhibit period bubbling behavior.

The paper is divided as follows. Section 2 concerns the description of the experimental setup. In section 3 we describe the theoretical models and compare them with the experimental results. In the last section we give the conclusions.

2.EXPERIMENTAL SETUP AND RESULTS

The experimental measurements have been performed with a laser cavity defined by a grating and a 90% reflectivity mirror with a radius of curvature of 3m placed 1.35 m apart. The laser is operated with a flowing gas mixture of CO_2≈9% vol., N_2≈12% vol., and He≈79% vol., at a total pressure of 20 Torr. The active medium excitation is obtained via a current stabilized longitudinal DC discharge at a fixed current value of 5.0 mA.

An intracavity electro-optic modulator (EOM) modulates the intracavity

field transmission so that the cavity damping rate can be expressed as follows

$$K = \frac{c}{2L}\left(2T + (1-2T)\sin^2(\pi V(t)/V_\lambda) \right) \qquad (1)$$

where c is the speed of light, L is the cavity length, T=0.10 is the total transmission coefficient for a single pass, V_λ=4240 V and $V(t)=V_0+V_1\sin(2\pi ft)$ is the voltage applied to the EOM (V_0=700 V). Considering that $V(t)<<V_\lambda$ we can approximate the expression for K as

$$\begin{aligned} K &= k(1 + m\sin(2\pi ft)) \\ k &= \frac{c}{2L}\left(2T + (1-2T)(\pi V_0/V_\lambda)^2 \right) \\ m &= 2V_1/V_0 \frac{1}{1+\alpha} \\ \alpha &= \frac{2T}{1-2T}(V_\lambda/\pi V_0)^2 \end{aligned} \qquad (2)$$

$k=4.61\ 10^7 s^{-1}$ being the cavity damping rate when the modulation amplitude m is set to zero.

Working with a fixed modulation frequency, we have increased the modulation amplitude m by changing V_1. The subharmonic cascade in the laser signal leading to chaos has been characterized measuring the values of the control parameter V_1 at which successive bifurcations occur (see Table I). We have recorded three bifurcation sequences at f_1=90 kHz, f_2=100 kHz and f_3=110 kHz. At $f=f_2$ we have also recorded stroboscopic Poincarè sections of

the laser output intensity each with 64,000 periods.

On the other hand, by changing the modulation frequency f at a fixed value of m, we have characterized the period-bubbling phenomenon. The result of the measurement is reported in Table II.

3.THEORETICAL MODELS AND COMPARISON WITH EXPERIMENTS

If we consider the CO_2 molecule as a simple two-level system coupled with a resonant electric field, we can describe the laser dynamics (in the case of sinusoidal loss modulation) with two differential equations for the photon number n and the population inversion δ between the two resonant levels (2LM) (dot denotes the time derivative):

$$\begin{aligned} \dot{n} &= kn\left(\delta - (1 + m\sin(2\pi ft+\phi)) \right) \\ \dot{\delta} &= -\gamma\delta - 2kn\delta + \gamma GP/k \end{aligned} \qquad (3)$$

n and δ have been renormalized to the steady state inversion when m=0, γ is the inversion decay rate (for the 2LMS $\gamma=1.95\ 10^4 s^{-1}$, for 2LME $\gamma=1.95\ 10^5 s^{-1}$ [5]), $G=9.9\ 10^{-8} s^{-1}$ is the field-matter coupling constant, $P=1.44\ 10^{14}$ is the pump parameter and ϕ is the phase shift. Values of G and P are rescaled from those given in Ref. 5.

As a matter of fact, the above description can be considerably improved taking into account the collisional coupling of each resonant level with a certain number Z of rotational levels of the same vibrational band (4LM). These considerations lead to a set of five differential equations for the

photon number n, the population inversion δ and the population sum σ of the resonant levels, and the population inversion Δ and the population sum Σ of the rotational manifolds.

$$
\begin{aligned}
\dot{n} &= kn\left(\delta - (1 + m\sin(2\pi ft+\phi))\right)\\
\dot{\delta} &= -\Gamma'\delta + \gamma\sigma + \gamma_R'\Delta - 2kn\delta + \gamma_2 GP/k\\
\dot{\sigma} &= -\Gamma\sigma + \gamma\delta + \gamma_R'\Sigma + \gamma_2 GP/k \qquad (4)\\
\dot{\Delta} &= -\Gamma'\Delta + \gamma\Sigma + \gamma_R\delta + \gamma_2 GZP/k\\
\dot{\Sigma} &= -\Gamma'\Sigma + \gamma\Delta + \gamma_R\sigma + \gamma_2 GZP/k
\end{aligned}
$$

All the variables have been rescaled with the steady state inversion of the resonant levels when m=0. The number of rotational levels considered in each manifold is Z=10. The decay rates Γ, Γ' and γ are defined as follows

$$
\begin{aligned}
\Gamma &= (\gamma_1 + \gamma_2)/2 + \gamma_R\\
\Gamma' &= (\gamma_1 + \gamma_2)/2 + \gamma_R' \qquad (5)\\
\gamma &= (\gamma_1 - \gamma_2)/2
\end{aligned}
$$

where γ_R=7.0 $10^6 s^{-1}$, γ_R'=7.0 $10^5 s^{-1}$, γ_1=8.0 $10^4 s^{-1}$, and γ_2=1.0 $10^4 s^{-1}$, according to the considerations given in Ref.[5]. The other parameters are the same as in the two-level model.

In what follows we will compare the two- and the four-level models with the experimental results of the previous section by using bifurcation diagram analysis. Once we show that the four-level model is the most suitable one, we further study it in terms of Poincaré sections and return

maps.

In Fig. 1a we report the bifurcation diagram for 4LM at a fixed value of the modulation frequency f=100 kHz. It can be verified that the numerical results are in good agreement with the experiment (the same agreement has been found at f=90 kHz and f=110 kHz). In fig.1b we report the bifurcation diagram at a fixed value of the modulation amplitude m=0.11. For this value of m the subharmonic window is bounded between 50 and 200 kHz. In Fig. 1c we report the primary bubble in 4LM at m=0.05 as the frequency is scanned.

In Fig. 2a we report the bifurcation diagram for 2LME at a fixed modulation frequency f=100 kHz. Comparing Figs. 1a and 2a we observe that 4LM is more easy to destabilize than 2LME. As we may see in 4LM (Fig. 1a) upon change of m, after the first continuous chaotic region a new chaotic attractor is originated from a period-3 unstable orbit. This crisis also occurs for m≈0.15 upon change of f and the attractor may be periodic or chaotic depending on f. A similar situation occurs for 2LME but for unphysical values of the parameters m and f. Figure 2b shows that, for the modulation amplitude m=0.11, the subharmonic region is shifted at frequencies higher than 120 kHz. 2LME also shows period bubbling for small values of m (≈0.05).

As regards 2LMS, the bifurcation diagram at f=100 kHz reported in Fig. 3a shows a continuous chaotic region which reminds roughly the bifurcation diagram of 4LM. The general difference is that successive crises in 2LMS are separated by small intervals of m in comparison with those of 4LM. In fig. 3b we see that for m=0.02 2LMS not only predicts chaos but also several crises as the frequency is scanned. The interval of modulation

frequencies where the subharmonics occur is roughly the same as in 4LM for small values of m, but period bubbling is not allowed due to the collision of the attractor (periodic orbit) with its basin boundary.

Comparing the numerical results of different models we can see that both the two-level models present relevant discrepancies with respect to 4LM. The main problem of 2LMS is the onset of chaos at low values of the modulation amplitude m [1]. One may think to improve this matter by increasing the decay rate γ thus increasing the value of m required to reach the chaotic regime. However as we have seen in 2LME, the price that one pays is that the frequency region where subharmonics appear is shifted far from that of the experiment. We have found these features also with the parameter set reported in Ref. 5.

We now compare the experimental Poincarè sections at the onset of chaos with those of the numerical simulations of 4LM. The projections of the numerical Poincarè section for period four in the plane (n,n) is shown in Fig. 4. Here we marked the order of the successive iterations. Figure 5 shows similar Poincarè sections at the onset of the chaotic regime (m=0.105 and f=100 kHz). Figure 4 suggests that the attractor represented in Fig. 5 consists of four pieces, which are visited in sequence. In fact, if we make a map by sampling the intensity or the inversion every four periods, we will find four different return maps.

As we may see in Fig. 5 a common feature of the return map is that a Cantor set structure (related to the horseshoe dynamics of the equations) occurs on a very fine scale and therefore an effective unidimensional map may represent the dynamics of the equations.

Two of the pieces of the map reported in Fig. 5 show a one to one correspondence between the points of the vertical and horizontal axes. Thus we construct the return map whenever the orbit is localized in one of these pieces, i.e. we form an unidimensional map by sampling the intensity or the intensity derivative every fourth iterate of the Poincarè map. In this way any two points lying in the same piece and with coordinates differing by a very small amount, will be mapped after four periods in other two close-lying points of that piece. The exponential divergence of the trajectories can be measured in terms of the Lyapunov exponent of the map [7] defined on that piece. One may observe parabola-like maps (Fig. 6a) until a crisis in the system appears. This crisis of the attractor is of the merging type since the four chaotic pieces are not anymore visited regularly. After the merging, the attractor is composed of two bigger pieces which in turn are visited regularly [10,12]. The corresponding return maps (shown in Fig. 6b for m=0.110 and f=100 kHz) may still be described as effective unidimensional maps which however have two extrema. This crisis occurs since the attractor touches the stable manifold of a saddle point generated in the process of saddle-node bifurcation as we change m [9].

In Fig. 7a and 7b we report the experimental return maps corresponding to Figs. 6a and 6b respectively. Here we point out that the attractor shown in Fig. 7a is sensitive to the noise present in the experiment so that it induces a merging of the two attractor pieces. After the merging, however, the attractor is more stable against noise (Fig. 7b).

We can now evaluate the Lyapunov exponent of the return maps reported in

Figs. 6b and 7b by fitting the theoretical and the experimental data with two polynomial curves $G(x)_{th}$ and $G(x)_{ex}$ respectively. The Lyapunov exponents of the maps are defined as follows [7]

$$\lambda_{th(ex)} = \lim_{N\to\infty} \frac{1}{N} \sum_{i}^{N} \ln \left| G'(x_i)_{th(ex)} \right|$$

Here N is the number of data points (N=2,500). The evolution of the Lyapunov exponents λ_{th} and λ_{ex} vs the number of data are shown in Figs. 8a and 8b respectively. The final values λ_{th}=0.762 and λ_{ex}=0.662 are in fair agreement. The correlation dimension calculations performed on the theoretical and experimental Poincaré sections confirm the low dimensionality of the attractor, giving values a few percent above one.

CONCLUSIONS

In the present paper we have shown that the four-level model is the only acceptable model to describe the chaotic behavior induced by losses modulation in a single mode CO_2 laser.

We have also established that for 4LM the period bubbling behavior persists beyond the values of the modulation parameters for the onset of chaos until crises arise. In 2LMS, even for values of m lower than those of 4LM, crises arise already in the periodic regime. In this way crises, which in turn are related to multistability, destroy period bubbling. In contrast, period bubbling is allowed in 2LME.

The treatment of the dynamics in terms of unidimensional maps has been possible, since just at the onset of chaos (reached by period doublings) any multidimensional system may be described as a noninvertible unidimensional map, and since period bubbling is an indication of low dimensionality. The theoretical analysis of the Poincarè maps shows the transition from maps with one extremum to maps with two extrema, as a consequence of a merging-type crisis.

In the experiment, due to the presence of noise which induces jumps between close lying orbits, we only observe maps with two extrema. However after the crisis, we find a fair agreement between the Lyapunov exponents calculated from the experimental and the numerical data.

ACKNOWLEDGEMENTS

This work was partly supported by the E.C. Contract N. SCI*-CT91-0697 (TSTS). C.L.P.L. is grateful for the hospitality of the Condensed Matter Group and Prof. H.Cerdeira at the International Center of Theoretical Physics (Trieste, Italy). The authors also thank Prof. G.Denardo for encouraging this work. He would also like to thank Professor Abdus Salam, the International Atomic Energy Agency, UNESCO and the International Centre for Theoretical Physics, for support.

REFERENCES

1 - F.T.Arecchi, R.Meucci, G.Puccioni and J.Tredicce, Phys. Rev. Lett. 49, 1217 (1982). G.Puccioni, A.Poggi, W.Gadomski, J.Tredicce and F.T.Arecchi,

Phys. Rev. Lett. 55, 339 (1985).

2 - J.Dupré, F.Meyer and C.Meyer, Rev. Phys. Appl. (Paris) 10, 285 (1975). E.Arimondo, F.Casagrande, L.A.Lugiato and P.Glorieux, Appl. Phys. B 30, 57 (1983).

3 - F.T.Arecchi, W.Gadomski, R.Meucci and J.R.Roversi, Optics Comm. 65, 47 (1988). G.-L.Oppo, J.R.Tredicce and L.M.Narducci, Optics Comm. 69, 393 (1989).

4 - V.Zehnle, D.Dangoisse and P.Glorieux, Optics Comm. 90, 99 (1992).

5 - R.Meucci, M.Ciofini and Peng-ye Wang, Optics Comm. 91, 444 (1992).

6 - G.-L.Oppo and A.Politi, Phys. Rev. A 30, 435 (1984). M.Bier and T.C.Bountis, Phys. Lett. 104A, 239 (1984).

7 - A.J.Lichtenberg and M.A.Lieberman, *Regular and stochastic motion*, Springer Verlag, Berlin (1983).

8 - E.Knobloch and N.O.Weiss, Physica 9D, 379 (1983); W.Krolikowski, M.R.Belic, M. Cronin-Golomb and A.Bledowski, J. Opt. Soc. B 7, 1204 (1990).

9 - J.M.T.Thompson and H.B.Steward, *Nonlinear Dynamics and Chaos*, Wiley New York, 1986.

10 - C.Grebogi, E.Ott and J.A.Yorke, Physica D 7, 181 (1983); Phys. Rev. Lett. 57, 1284 (1986).

11 - D.Hennequin, P.Glorieux and D.Dangoisse, Phys. Rev. Lett. 57, 2657 (1986). H.G.Solari, E.Eschenazi, R.Gilmore and J.R.Tredicce, Optics Comm. 64, 49 (1987). R.Meucci, A.Poggi, F.T.Arecchi and J.R.Tredicce, Optics Comm. 65, 151 (1988).

12 - C.Grebogi, E.Ott, F.Romeiras and J.Yorke, Phys. Rev. A 36, 5365 (1987).

TABLE CAPTIONS

Table I - Experimental bifurcation values of the parameters V_1 and m for three different modulation frequencies.

Table II - Experimental bifurcation values of the parameter f for V_1=73.5 V corresponding to m=0.108.

TABLE I

f (kHz)	V_1 (V)	m	onset of
90	33.6	0.050	f/2
	79.8	0.118	f/4
	88.5	0.131	chaotic f/8
	92.6	0.137	chaotic f/2
	94.5	0.140	chaos
	114.1	0.169	f/3
100	31.3	0.046	f/2
	71.7	0.106	f/4
	77.7	0.115	f/8
	83.6	0.124	chaotic f/2
	87.5	0.130	chaos
	103.6	0.153	chaotic f/3
110	34.3	0.051	f/2
	69.1	0.102	f/4
	78.0	0.115	f/8
	84.9	0.126	chaotic f/2
	92.4	0.137	chaos
	105.0	0.155	f/3

TABLE II

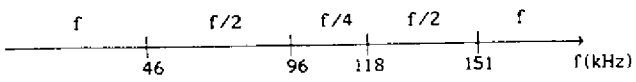

FIGURE CAPTIONS

Fig. 1 - Numerical results for 4LM. a) Bifurcation diagram for the inversion δ vs the modulation amplitude m at f=100 kHz. b) Bifurcation diagram of δ vs the modulation frequency f at m=0.11. c) The same as b) but for m=0.05.

Fig. 2 - Numerical results for 2LME. a) Bifurcation diagram of δ vs m at f=100 kHz. b) Bifurcation diagram for the inversion δ vs the modulation frequency at m=0.11.

Fig. 3 - Numerical results for 2LMS. a) Bifurcation diagram of δ vs m at f=100 kHz. a) Bifurcation diagram for the inversion δ vs the modulation frequency at m=0.02.

Fig. 4 - Poincaré map projection on the plane (n,n) at f=100 kHz and m=0.09 (period four).

Fig. 5 - The same as Fig. 4 but for m=0.105 (onset of chaos). The attractor merging of the "linear" pieces is shown (it is also observed in the other two pieces).

Fig. 6 - Return maps obtained with the fourth iterates of the photon number at f=100 kHz; a) m=0.105, b) m=0.110.

Fig. 7 - Experimental return maps for the laser intensity obtained with the fourth iterates at f=100 kHz. a) m=0.118, b) m=0.124.

Fig. 8 - Lyapunov exponents calculations for a) the return map of Fig. 6b (λ_{th}) and b) the return map of Fig. 7b (λ_{ex}).

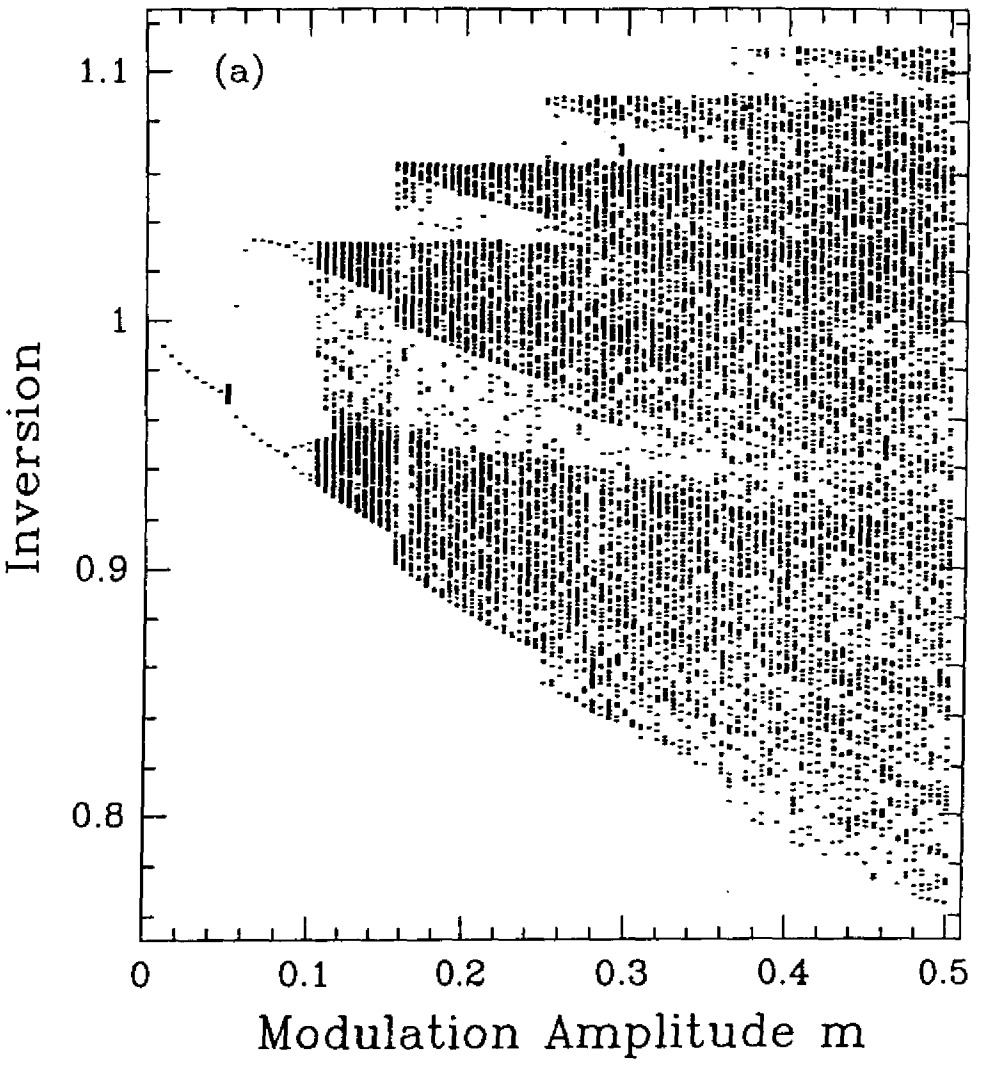

Fig.1a

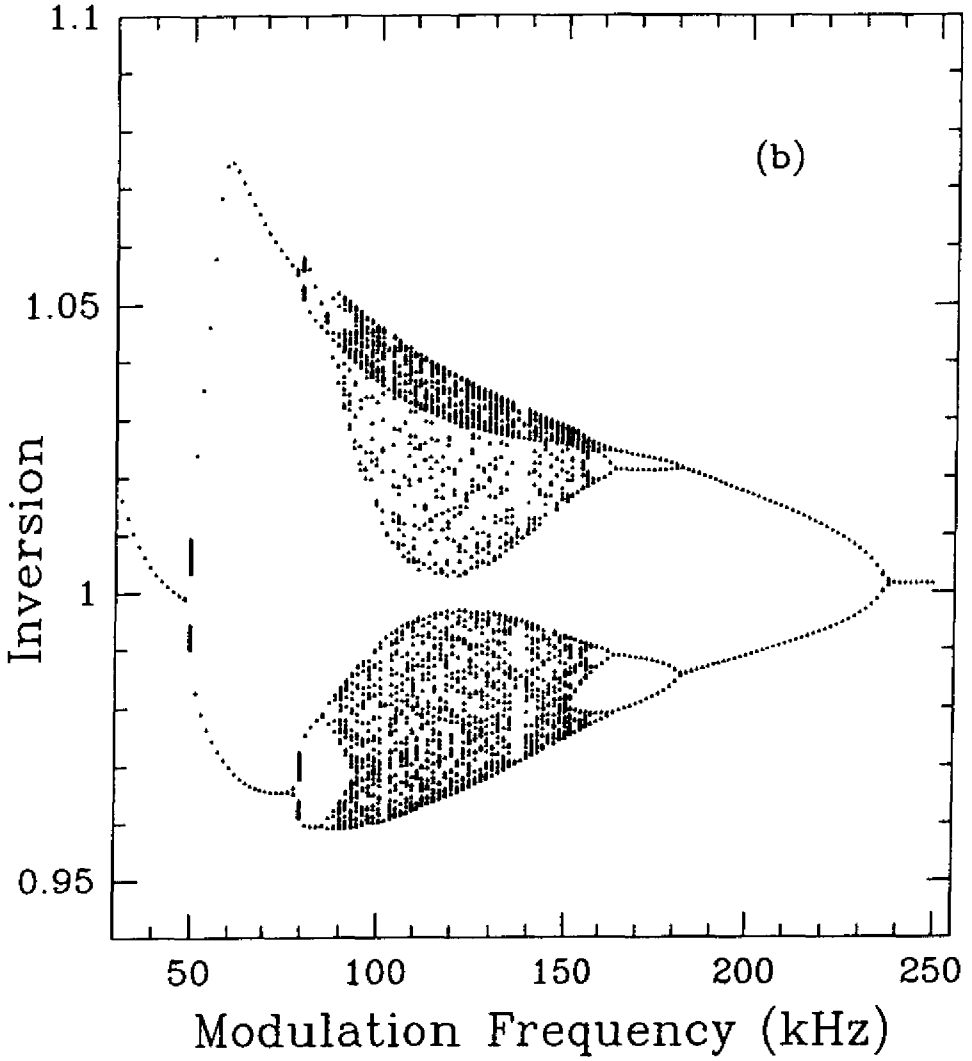
(b)
1.1
1.05
1
0.95
Inversion
50
100
150
200
250
Modulation Frequency (kHz)

Fig.1b

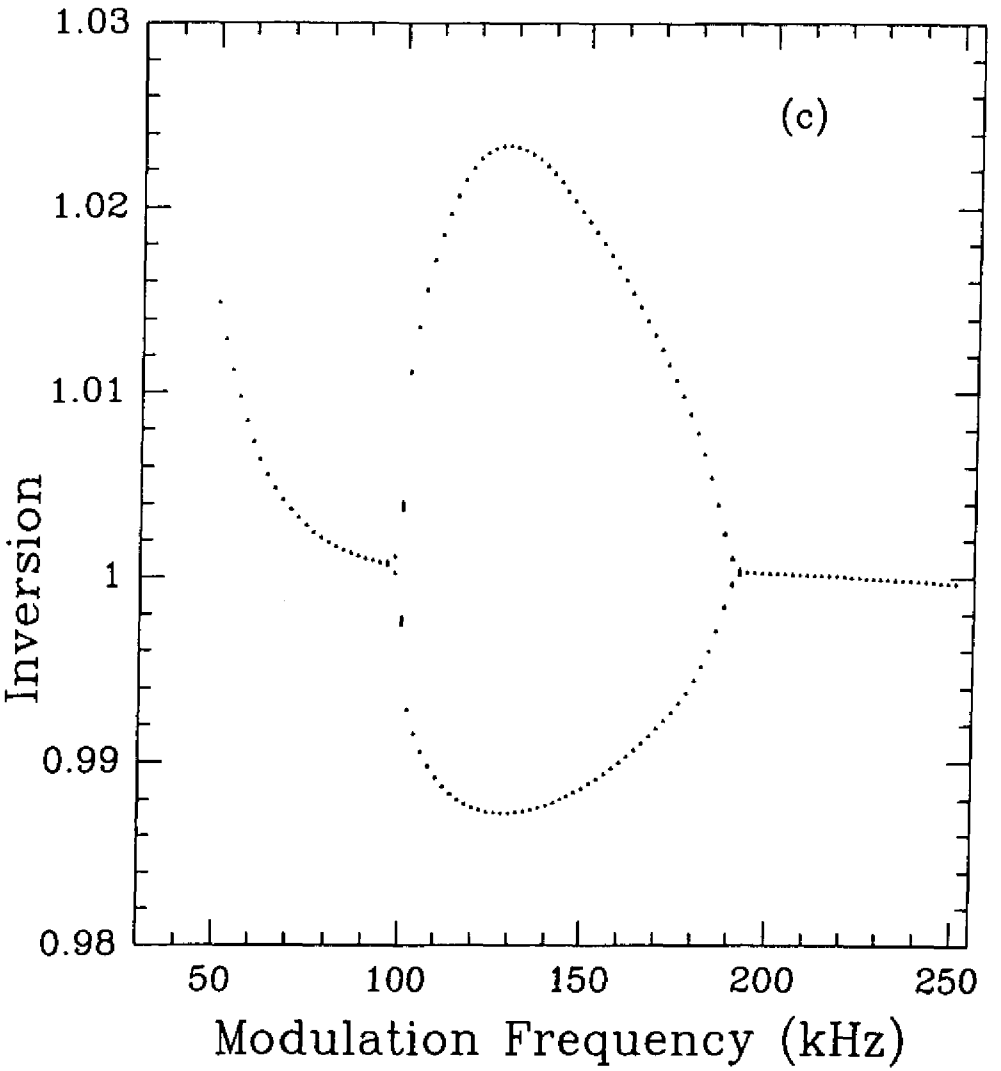
(c)
1.03
1.02
1.01
1
0.99
0.98
Inversion
50
100
150
200
250
Modulation Frequency (kHz)

Fig.1c

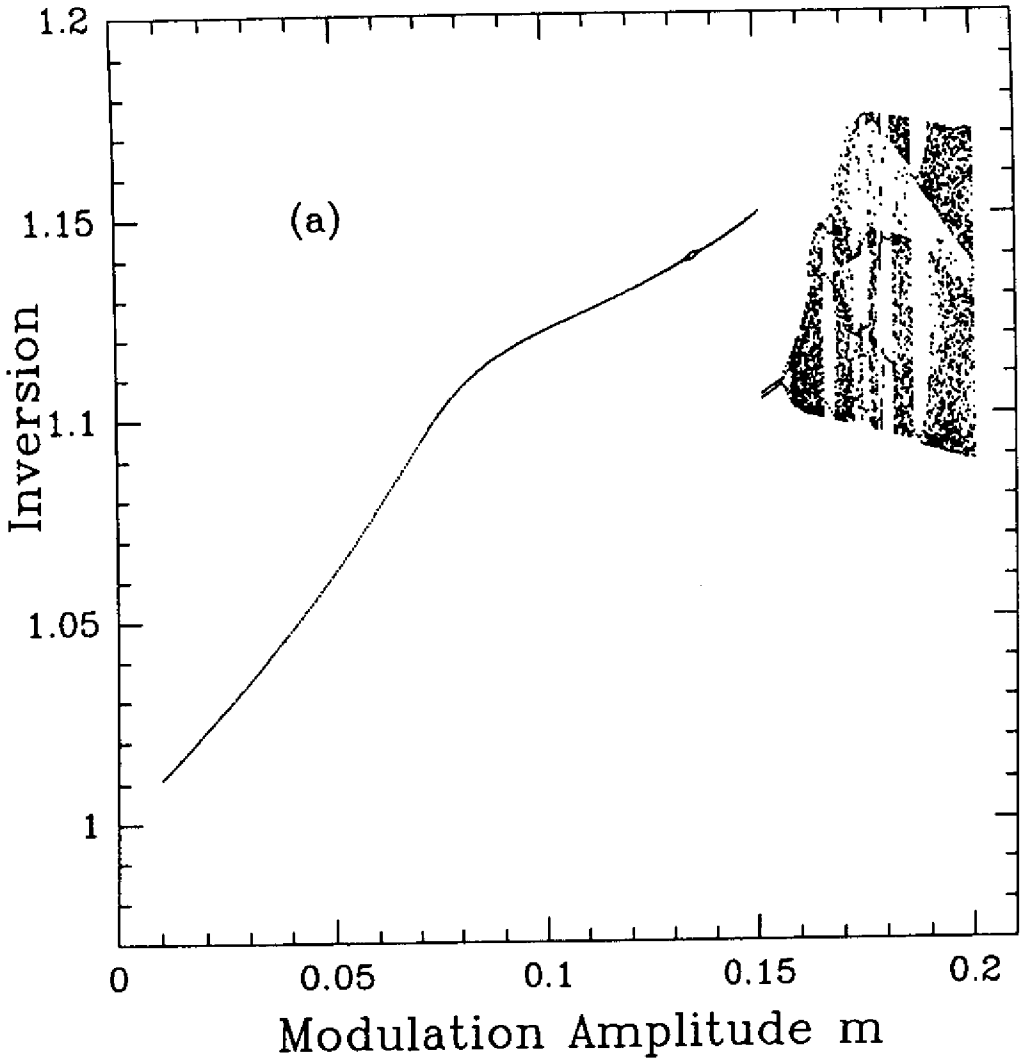
(a)
Inversion
1.2
1.15
1.1
1.05
1
0
0.05
0.1
0.15
0.2
Modulation Amplitude m

Fig.2a

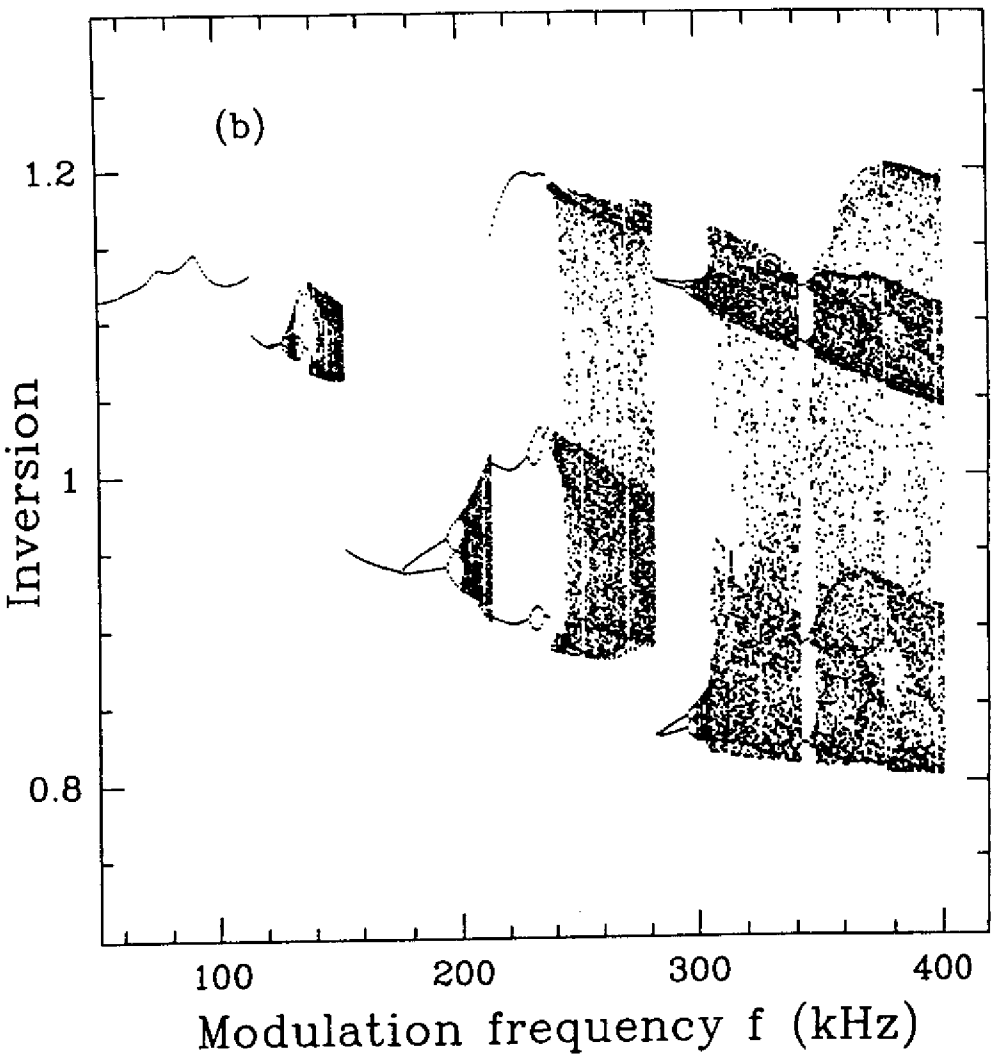
(b)
Inversion
1.2
1
0.8
100
200
300
400
Modulation frequency f (kHz)

Fig.2b

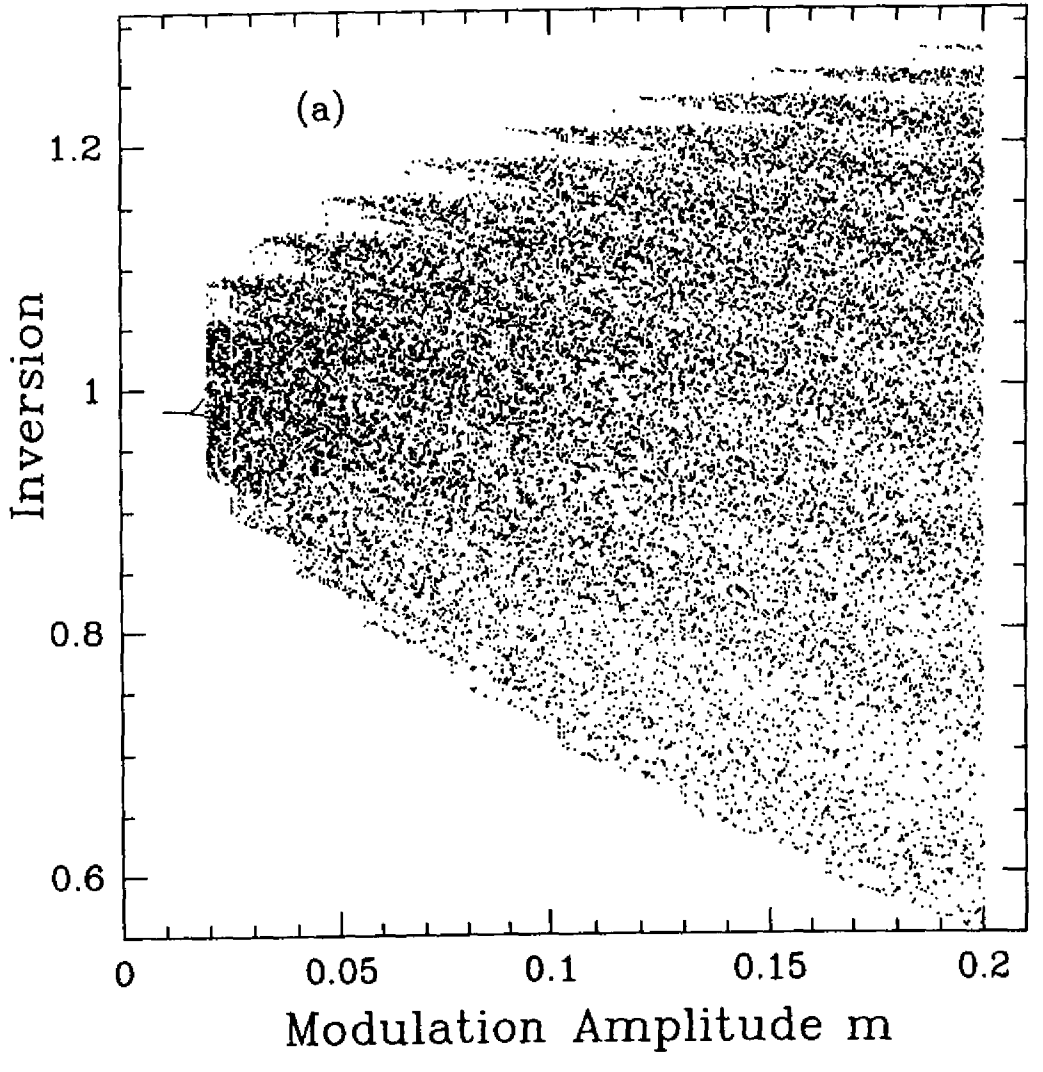
(a)
1.2
1
0.8
0.6
Inversion
0
0.05
0.1
0.15
0.2
Modulation Amplitude m

Fig.3a

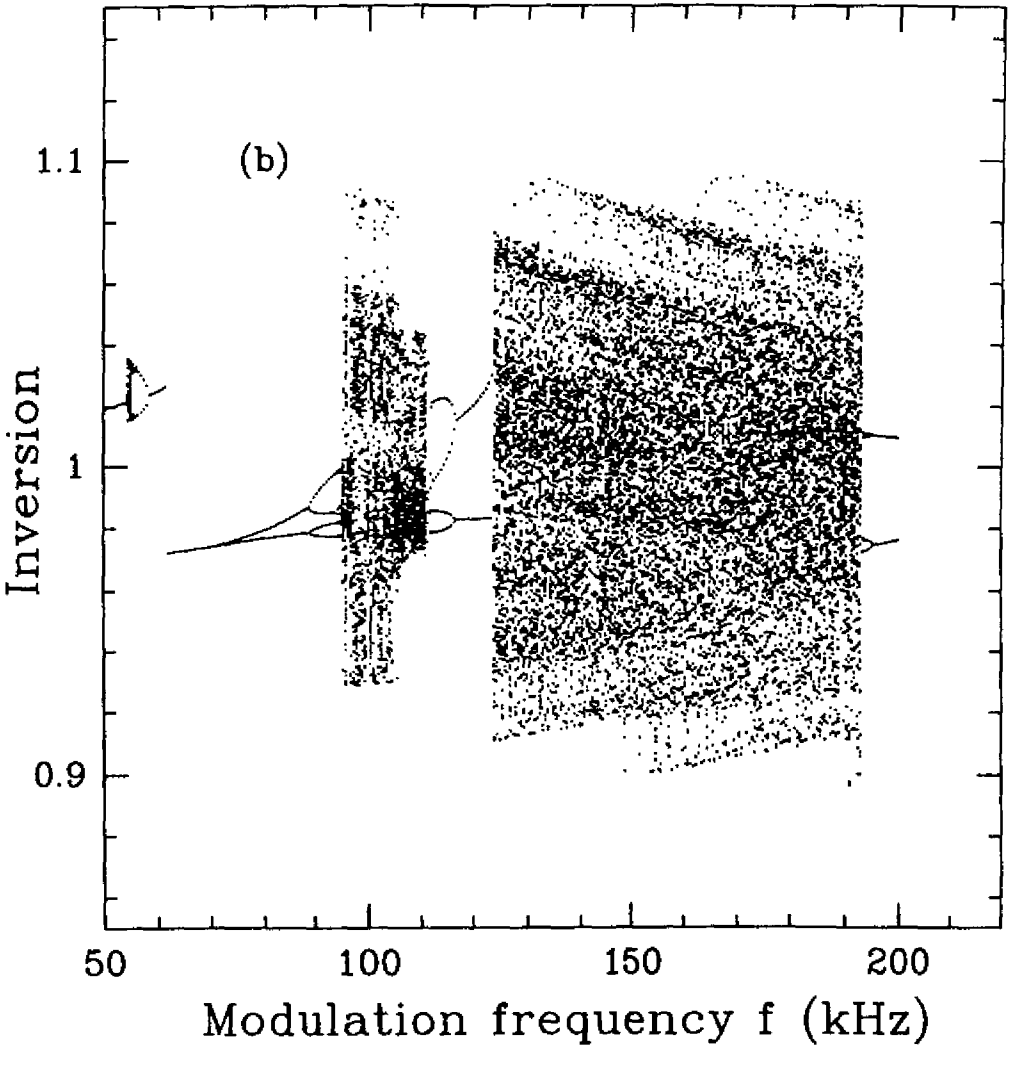
(b)
1.1
1
0.9
Inversion
50
100
150
200
Modulation frequency f (kHz)

Fig.3b

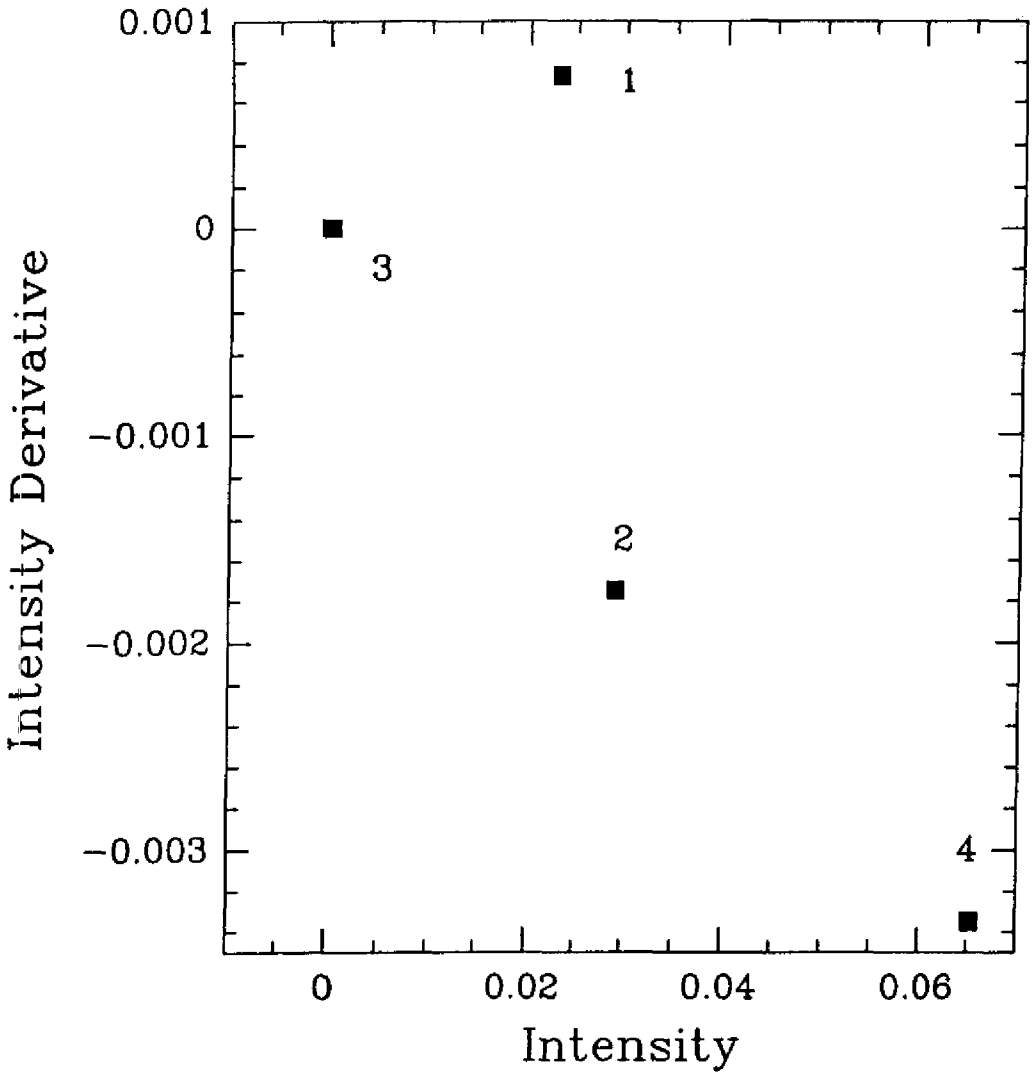
0.001
0
−0.001
−0.002
−0.003
Intensity Derivative
1
2
3
4
0
0.02
0.04
0.06
Intensity

Fig.4

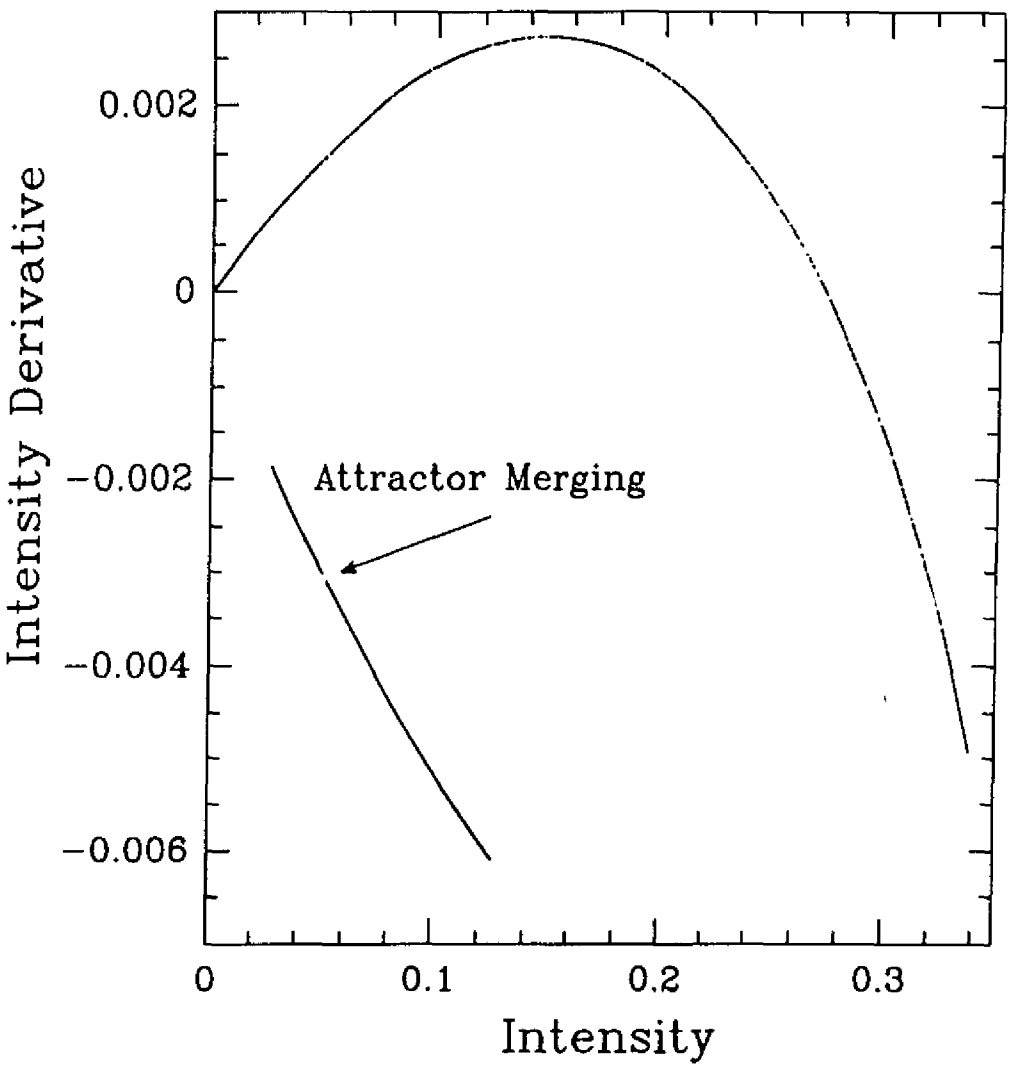
0.002
0
−0.002
−0.004
−0.006
Intensity Derivative
Attractor Merging
0
0.1
0.2
0.3
Intensity

Fig.5

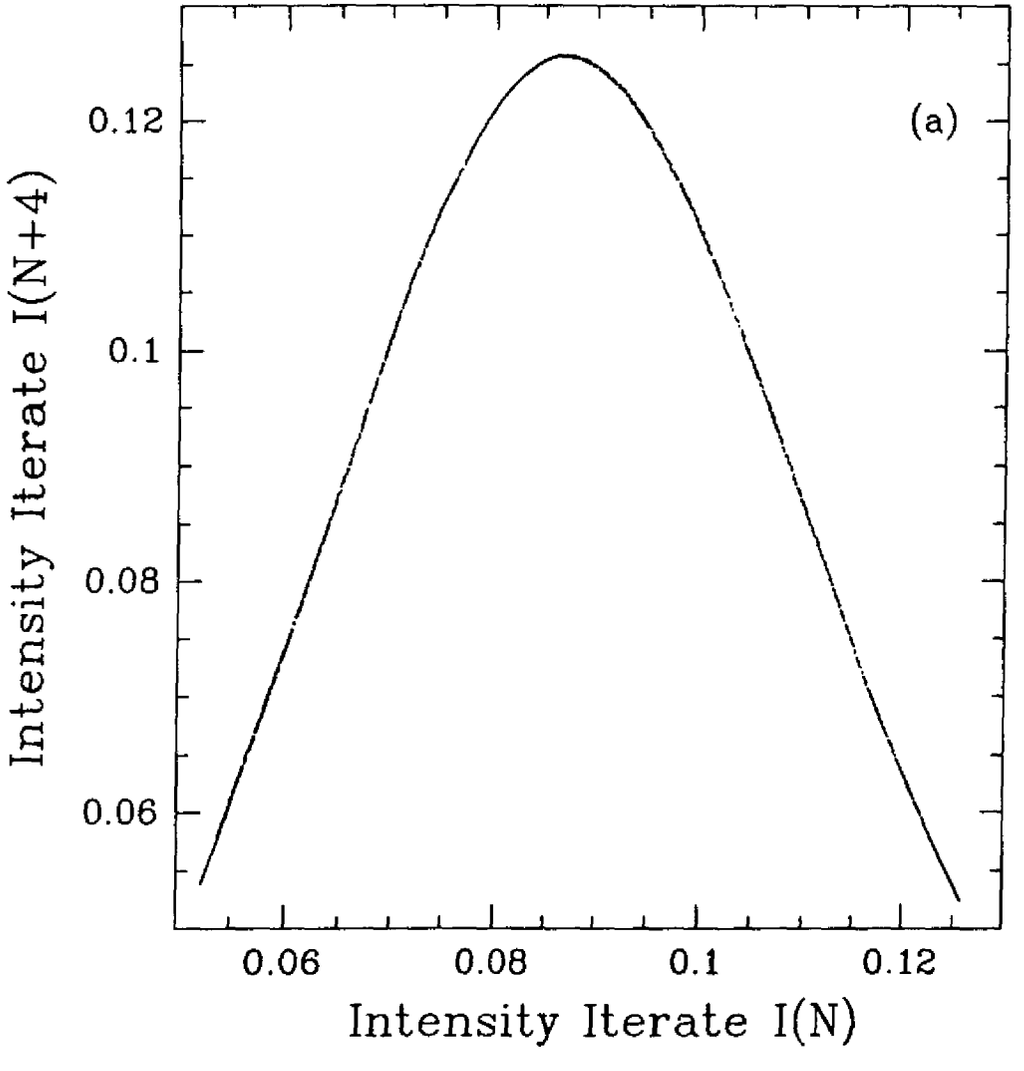
(a)
0.12
0.1
0.08
0.06
Intensity Iterate I(N+4)
0.06
0.08
0.1
0.12
Intensity Iterate I(N)

Fig.6a

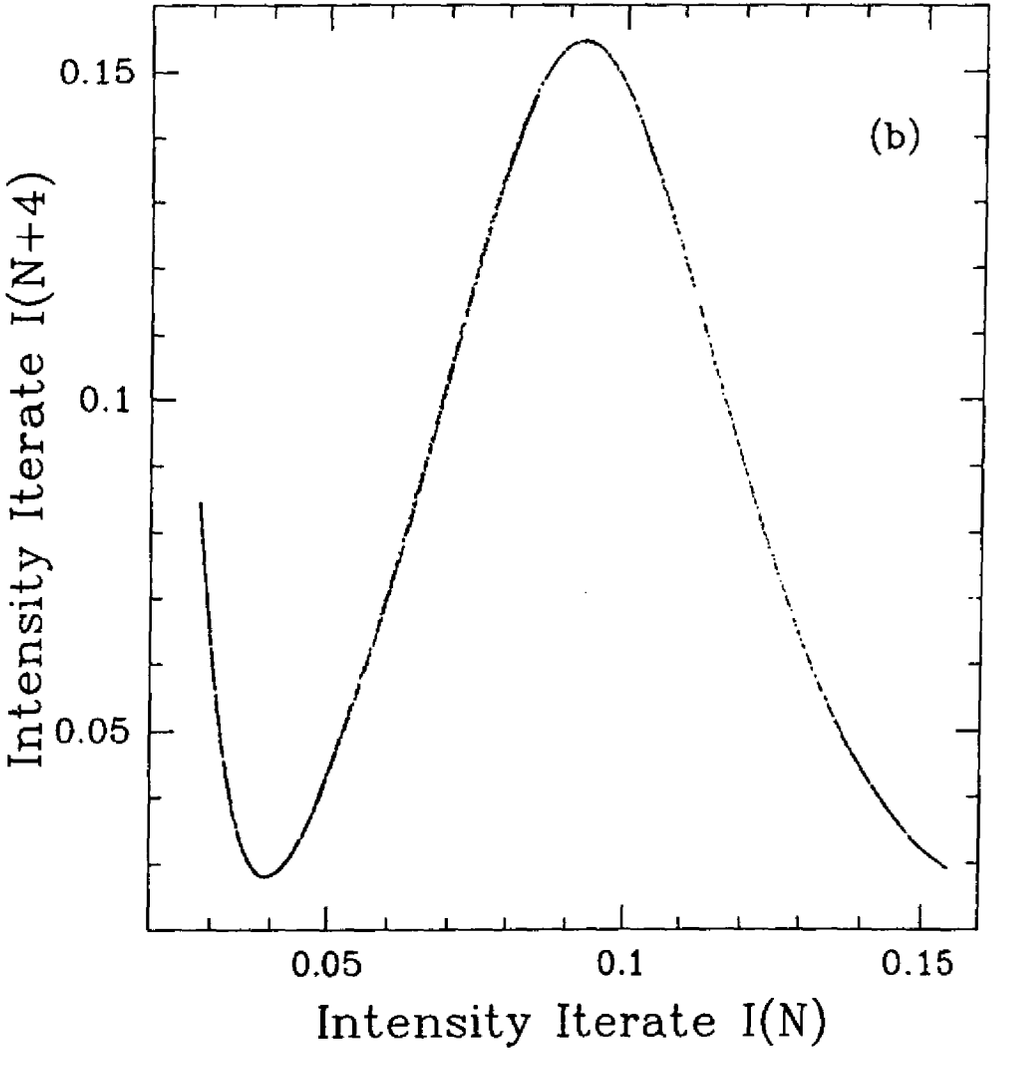
(b)
0.15
0.1
0.05
Intensity Iterate I(N+4)
0.05
0.1
0.15
Intensity Iterate I(N)

Fig.6b

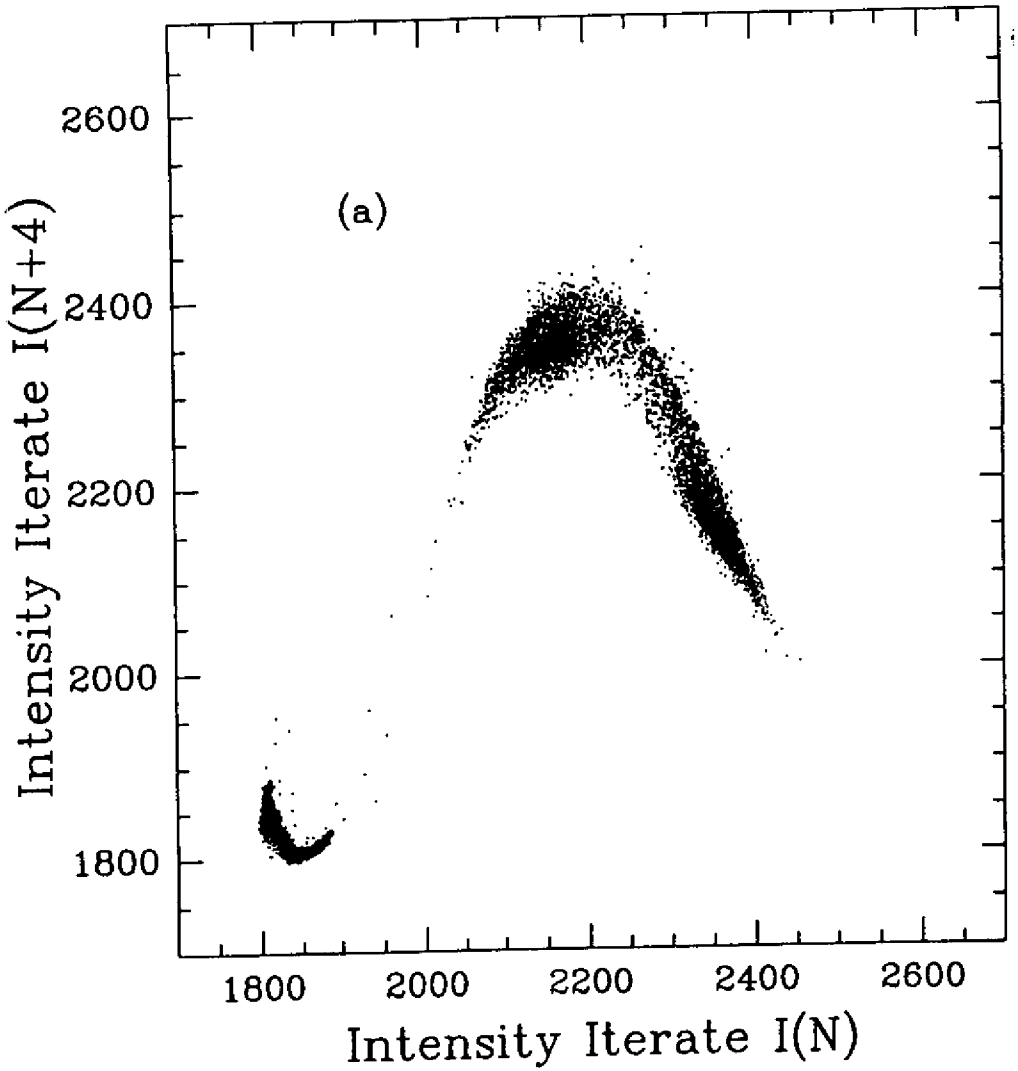
(a)
Intensity Iterate I(N+4)
Intensity Iterate I(N)
2600
2400
2200
2000
1800
1800
2000
2200
2400
2600

Fig.7a

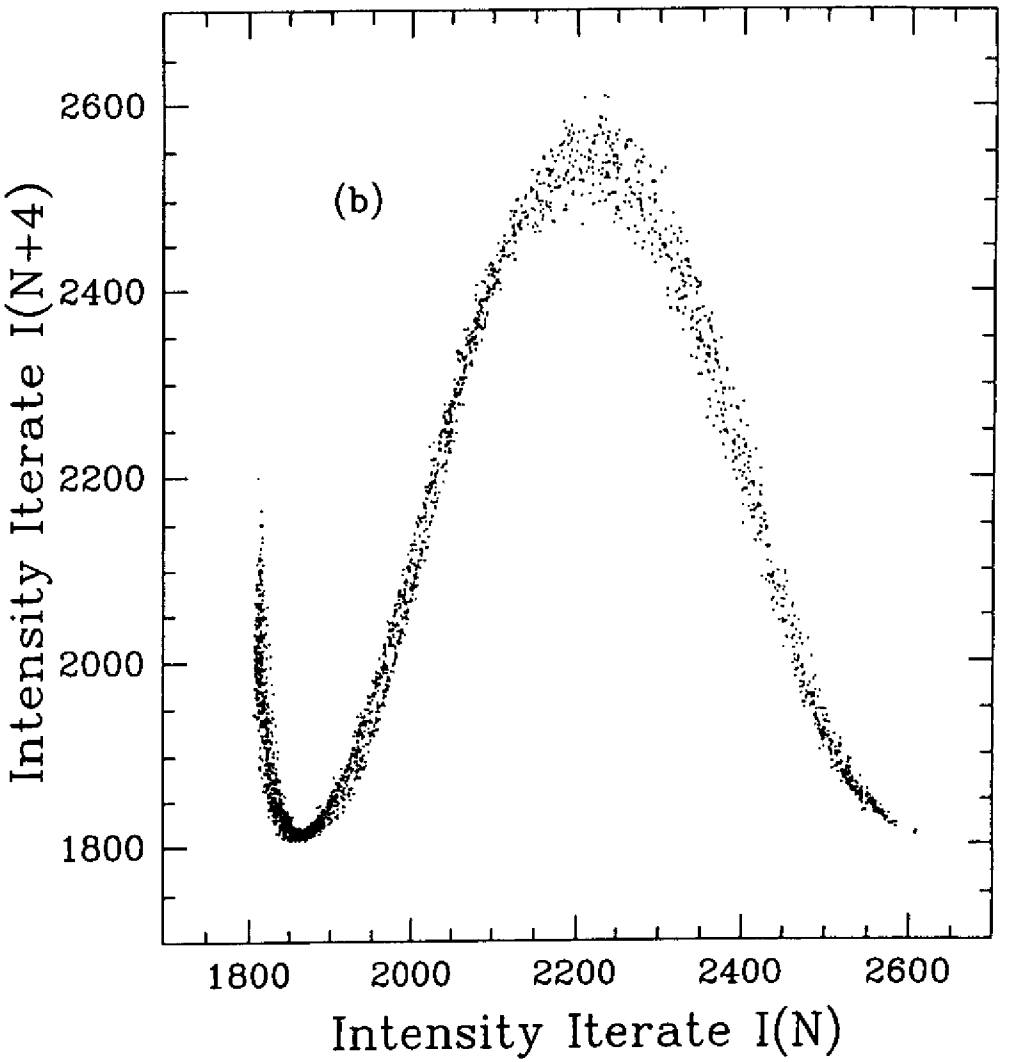
(b)
Intensity Iterate I(N+4)
Intensity Iterate I(N)
2600
2400
2200
2000
1800
1800
2000
2200
2400
2600

Fig.7b

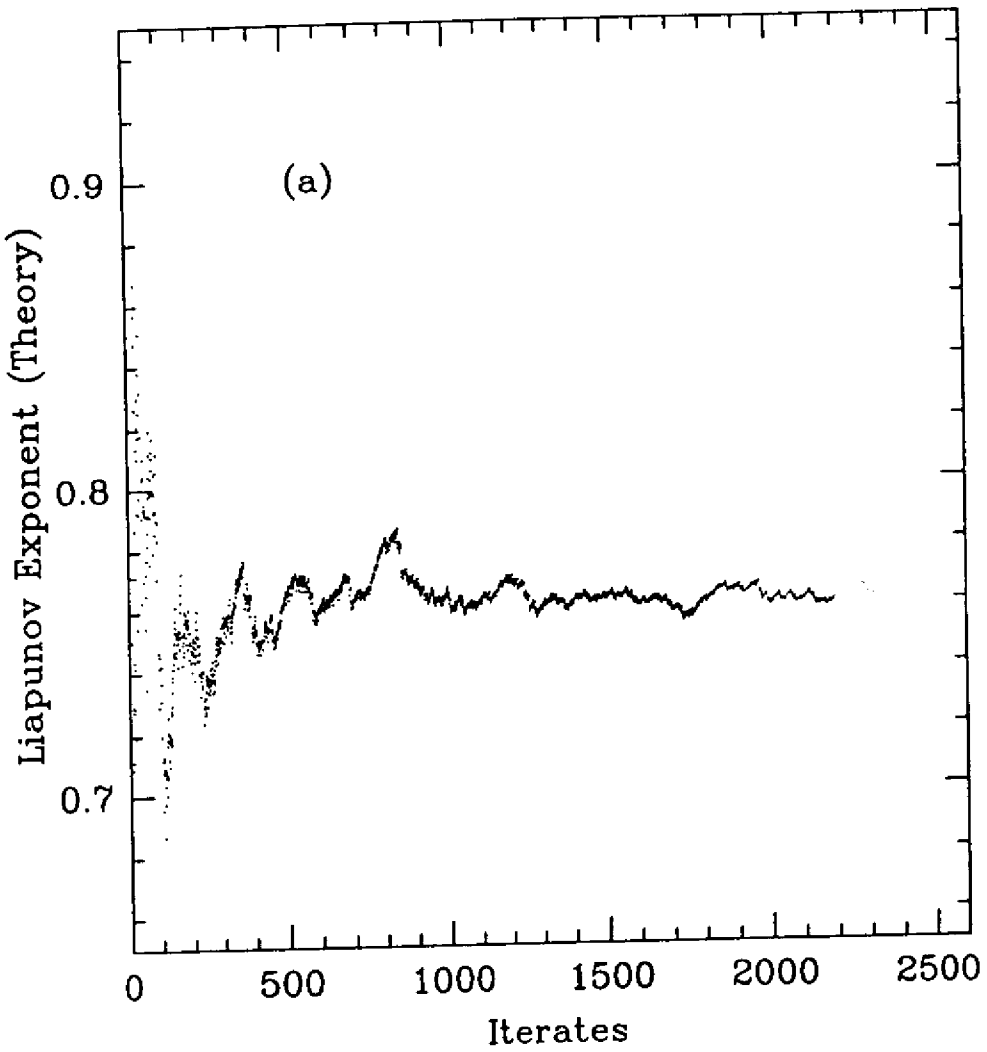
(a)
Liapunov Exponent (Theory)
0.9
0.8
0.7
0
500
1000
1500
2000
2500
Iterates

Fig.8a

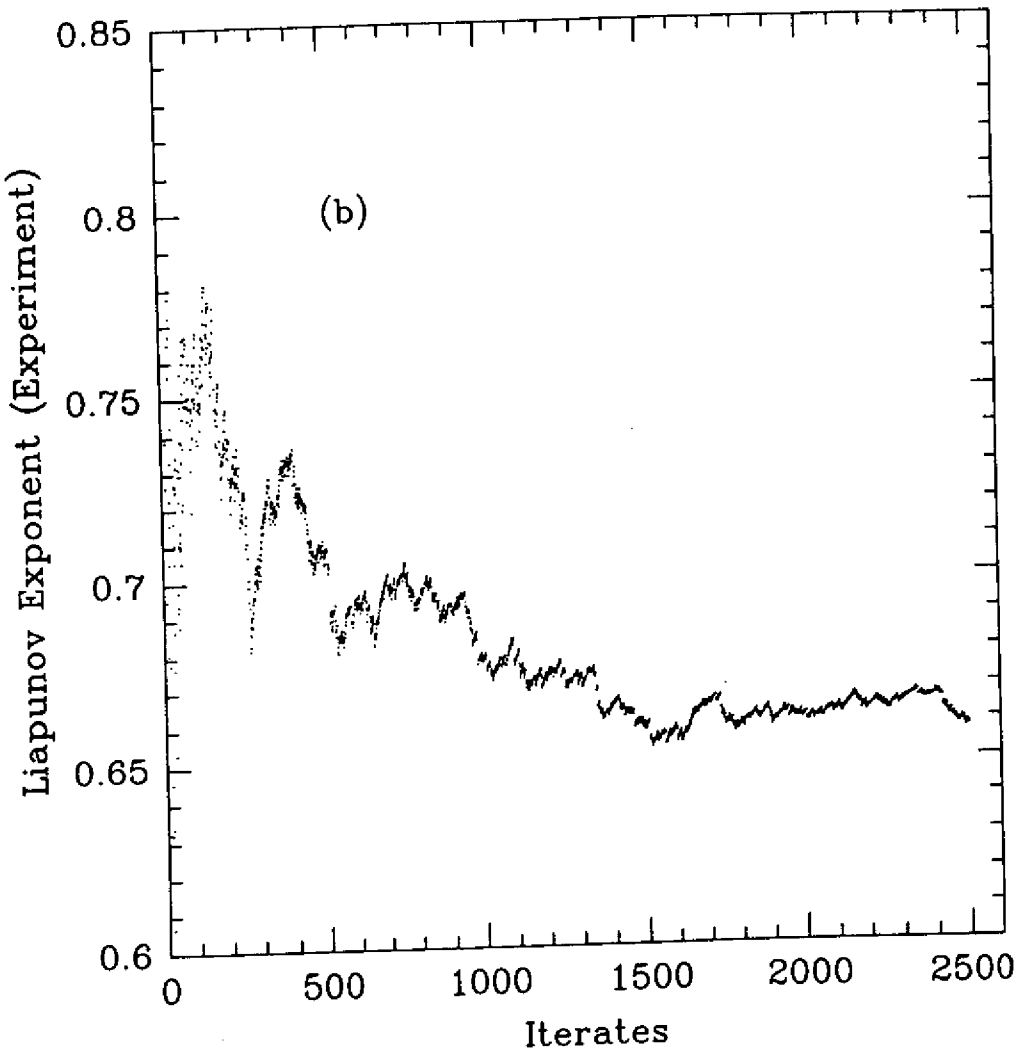
(b)
Liapunov Exponent (Experiment)
0.85
0.8
0.75
0.7
0.65
0.6
0
500
1000
1500
2000
2500
Iterates

Fig.8b